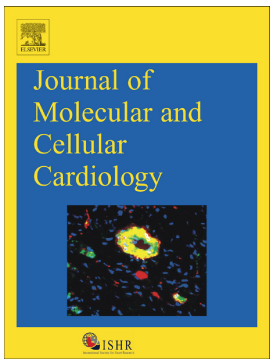

Novel anti-aging gene NM_026333 contributes to proton-induced aging via NCX1-pathway

Tomohiro Osanai, Makoto Tanaka, Kasumi Mikami, Maiko Kitajima, Toshiko Tomisawa, Koji Magota, Hirofumi Tomita, Ken Okumura

PII: S0022-2828(18)30553-4
DOI: doi:10.1016/j.yjmcc.2018.10.021
Reference: YJMCC 8839

To appear in: *Journal of Molecular and Cellular Cardiology*

Received date: 14 July 2018
Revised date: 4 October 2018
Accepted date: 25 October 2018

Please cite this article as: Tomohiro Osanai, Makoto Tanaka, Kasumi Mikami, Maiko Kitajima, Toshiko Tomisawa, Koji Magota, Hirofumi Tomita, Ken Okumura , Novel anti-aging gene NM_026333 contributes to proton-induced aging via NCX1-pathway. Yjmcc (2018), doi:10.1016/j.yjmcc.2018.10.021

Novel anti-aging gene NM_026333 contributes to proton-induced aging via NCX1-pathway

Tomohiro Osanai, MD[1,2,3,4,5,*] osanait@hirosaki-u.ac.jp, Makoto Tanaka, MD[2], Kasumi Mikami, RN PhD[1,2,3,4,5], Maiko Kitajima, RN PhD[1,2,3,4,5], Toshiko Tomisawa, RN PhD[1,2,3,4,5], Koji Magota, PhD[4], Hirofumi Tomita, MD[3], and Ken Okumura, MD[5]

[1]Department of Nursing Science, Hirosaki University Graduate School of Health Science, Hirosaki, Japan

[2]Department of Hypertension and Stroke Internal Medicine, Hirosaki University Graduate School of Medicine, Hirosaki, Japan

[3]Department of Cardiology, Hirosaki University Graduate School of Medicine, Hirosaki, Japan

[4]Daiichi Sankyo Co., Ltd., Biologics Technology Research Laboratories Group1, Pharmaceutical Technology Division, 2716-1, Kurakake, Akaiwa, Chiyoda-machi, Oura-gun, Gunma 370-503, Japan

[5]Saiseikai Kumamoto Hospital, Division of Cardiology, Kumamoto, Japan

The authors have declared that no conflict of interest exists

*Corresponding author at: Department of Nursing Science, Hirosaki University Graduate School of Health Science 66-1 Hon-cho, Hirosaki, 036-8564 Japan.

Abbreviations

TG	Transgenic
CF6	Coupling factor 6
NCX1	Na^{+}-Ca^{2+} exchanger 1
HDAC1-4	Histone deacetylase 1-4
H4K5ac, H4K8ac, H4K12ac	Acetyl-histone 4 at lysine 5, 8, and 12
H3K4/9/27me3, H4K20me3	Histone 3/4 at lysine 4/9/27/20 trimethylation
HP1α	Heterochromatin protein 1α
HMGB1	High-mobility group box 1
BAF	Barrier-to-autointegration factor
TRPC3	Transient receptor potential C3
FBS	Fetal bovine serum
SSC	Sodium chloride and sodium citrate
SDS	Sodium dodecyl sulfate
ChIP	Chromatin immunoprecipitation
ANOVA	Analysis of variance
LC3 II	LC3 phosphatidylethanolamine
Chk1	Checkpoint kinase 1

CACNA2D2	Volyage-gated calcium channel UNC-36
SLC7A6	Cationic amino acid transporter

ABSTRACT

Diet-induced metabolic acidosis is associated with the impairment of bone metabolism and an increased risk of a number of chronic noncommunicable diseases, such as type 2 diabetes mellitus and hypertension. Low serum bicarbonate is associated with high mortality in healthy older individuals. Recently, we demonstrated that both coupling factor 6 (CF6)-overexpressing transgenic (TG) and high salt-fed mice which had sustained intracellular acidosis, due to enhanced proton import through ecto-F_1F_o complex and/or reduced proton export through Na^+-K^+ ATPase inhibition, displayed shortened lifespan and early senescence-associated phenotypes such as signs of hair greying and alopecia, weight loss, and/or reduced organ mass. In this study, we searched causative genes of proton-induced aging in CF6-overexpressing TG and high salt-fed mice. We discovered NM_026333 as a novel anti-aging gene which was downregulated in the heart and kidney in both types of mice. NM_026333 protein consists of 269 amino acids with transmembrane region (90-193aa). Induction of NM_026333 or recombinant protein rescued TG cells and CF6-treated human cells from aging hallmarks of impaired autophagy, genomic instability, and epigenetic alteration. NM_026333 protein directly bound plasma membrane Na^+-Ca^{2+} exchanger 1 (NCX1) to suppress its reverse mode, and cancelled proton-induced epigenetic regression of Atg7

that was caused by H3K4 and H4K20 tri-methylation via suppression of demethylase and H4K5 acetylation via suppression of nuclear HDAC3-HDAC4-emerin system. NM_026333 also attenuated proton-induced impaired formation of autolysosome, an increase in nuclear acetylated LC3 II, and acetylation of Atg7. These effects reappeared by NCX1 inhibitor. Furthermore, NCX1 inhibitor extended lifespan compared with vehicle-treatment in TG mice. This study will shed light on novel aging mechanism and provide implications in a target for anti-aging therapy.

Keywords: anti-aging gene, coupling factor 6, epigenetics, autophagy, genomic instability, NCX1

INTRODUCTION

Aging is characterized by a progressive loss of physiological integrity. A number of factors contribute to the aging process and phenotype (1). Cellular senescence, reactive oxygen species, and optimal nutrient sensing accelerate aging at high levels, but mediate beneficial effects at low levels, indicating usefulness of caloric restriction (2) and removal of senescent cells (3) as anti-aging therapy. In contrast, genomic instability, telomere attrition, epigenetic alterations, and defective proteostasis are the initiating triggers whose damaging events accumulate with time (1). Diet-induced metabolic acidosis has been reported to be associated with the impairment of bone metabolism and an increased risk of a number of chronic noncommunicable diseases, such as type 2 diabetes mellitus and hypertension (4-6). Low serum bicarbonate is associated with high mortality in healthy older individuals (7). Recently, we demonstrated that both coupling factor 6 (CF6)-overexpressing transgenic (TG) and high salt-fed mice which had sustained intracellular acidosis, due to enhanced proton import through ecto-F_1F_o complex and/or reduced proton export through Na^+-K^+ ATPase inhibition, displayed shortened lifespan and early senescence-associated phenotypes such as signs of hair greying and alopecia, weight loss, and/or reduced organ mass (8,9).

We previously identified CF6 as a ligand for ecto-F_1F_o complex, and after binding

to protrusive F_1, CF6 forces the backward rotation of F_o, thereby stimulating proton import at the plasma membrane (10). The whole F_1F_o-ATP synthase complex localizes on the outer surface of the plasma membrane in various cells. In the plasma membrane, F_1 can hydrolyze ATP and inversely rotate F_o to pump protons in the opposite direction when the free energy of ATP hydrolysis is large in the extracellular space, leading to intracellular acidosis. CF6 has been disclosed to exert a widespread action of vascular biology such as inhibition of prostacyclin and platelet endothelial cell adhesion molecule 1, and stimulation of endogenous nitric oxide synthases inhibitor asymmetric dimethyl arginine (11-17). In the clinical settings, we and others showed that circulating CF6 is elevated in patients with end-stage renal disease, myocardial infarction, stroke, hypertension, and diabetes (18-21), all of which are aging-related diseases. Overall, identification of a key molecule related to CF6-induced and proton-induced accelerated aging might shed light on novel aging mechanism and provide implications in a target for anti-aging therapy.

In the present study, we searched causative genes of proton-induced aging in CF6-overexpressing TG and high salt-fed mice. We discovered NM_026333 as a novel anti-aging gene which was commonly downregulated in the heart and kidney in both types of mice. Induction of NM_026333 or recombinant protein rescued TG cells from

aging hallmarks of impaired autophagy, genomic instability, and epigenetic alterations

Materials and Methods

Materials

Effectene Transfection Reagent, QIA shredder, and RNeasy Protect Mini Kit were from QIAGEN, Valencia, CA, USA. Gibco DMEM, FBS, and penicillin/streptomycin were from Life technology corporation. Amino Allyl MessageAmp^{TM} aRNA kit was from Ambion, TX, USA. Human CF6 was from Phoenix Pharmaceuticals, Inc., Belmont, CA, USA. RIPA lysis buffer, antibody for GAPDH, and mouse monoclonal antibody for emerin were from Santa Cruz Biotechnology, Santa Cruz, California, USA. Antibodies for human histone deacetylase 1-4 (HDAC1-4), acetyl-histone 4 at lysine 5, 8, and 12 (H4K5, H4K8, H4K12), and tri-methylation of H3K4, K9, K27, and H4K20, lamin A/C, heterochromatin protein 1α (HP1α), high-mobility group box 1 (HMGB1), barrier-to-autointegration factor (BAF), p62, and Atg7 were from Cell Signaling Technology, Inc., Danvers, MA, USA. Antibodies for pan-acetyl histone 3 and 4 were from Active Motif Inc., Tokyo, Japan. Mouse monoclonal antibody for LC3 was from Cosmo Bio Co., Ltd, Tokyo, Japan. Rabbit polyclonal antibody for Lamp 1 was from Abcam, Tokyo, Japan. Rabbit polyclonal antibodies for Na^{+}-Ca^{2+} exchanger 1 (NCX1),

transient receptor potential C3 (TRPC3) and TRPC6, and Cav1.2 were from Alomone Labs, Jerusalem, Israel. TALON magnetic beads (Cat. Nos. 635636 & 635637) and Talon magnetic beads buffer kit were from Clontech Laboratories, Inc., Mountain View, CA, USA. SN-6 was from Tocris Bioscience, Avonmouth, Bristol, BS11 9QD, United Kingdom. ReadyPrep protein extraction kit (cytoplasmic/nuclear) was from Bio-Rad Laboratories, Inc., Hercules, CA, USA. TransIT-293 Transfection Reagent was from Mirus Bio LLC, Madison, WI, USA. Fura-2 AM and Dapi were from DOJINDO Laboratories, Kumamoto Japan. Ionomycin was from Calbiochem, La Jolla, CA, USA. Texas Red, FITC-Goat-Anti-rabbit IgG, FITC-rabbit-anti-mouse IgG, and Lipofectamine 3000 Transfection Kit (L3000-015) were from Invitrogen Corporation, Carlsbad, CA, USA. Alexa Fluor 488 (A11055) and Alexa Fluor 568 (A10042) were from Thermo Fisher Scientific, Waltham, MA. Picagene Luciferase Assay System was from Toyo Ink, and Galacto-Light Plus System was from Applied Biosystems. Luciferase reporter vector was from Picagene basic vector, Toyo Ink Mfg. Co., Ltd., Tokyo, Japan. Galacto-Light Plus System was from Applied Biosystems, Thermo Fisher Scientific, Waltham, MA. AceGene-Mouse Oligo Chip 30K 1 Chip Version was from Hitachi Software Engineering Co.,Ltd. Kanagawa, Japan. Cy3- or Cy5-conjugated deoxyribonucleotides were from Amersham Biosciences, Germany. Polyvinilidene

difluoride membrane was from Bio-Rad Laboratories, Hercules, California, USA. Enhanced chemiluminescence plus detection systems were from Amersham Pharmacia Biotech, Piseataway, New Jersey, USA. All other reagents were of the finest grade available from Sigma Chemical Co., St. Louis, Missouri, USA.

Cell culture

Primary mouse cardiac fibroblasts from CF6-overexpressing mice and wild type mice and HEK-293 or C2C12 cells were cultured in DMEM supplemented with 10% fetal bovine serum (FBS), 100 U/ml penicillin, and 100 μg/ml streptomycin at 37 °C under 5% CO_2. Fibroblasts from the second to seventh passages were used.

RNA Isolation

The tissues and cells were rinsed quickly in ice-cold PBS and RNA was isolated by using RNeasy® Mini Kit according to the manufacturer's instructions. RNA quality was insured by spectrophotometric analysis (OD260/280). The RNA was quantitated by spectrophotometric analysis at 260 nm. Linear amplification of mRNA from total RNA was obtained using the Amino Allyl MessageAmp^{TM} aRNA kit with two consecutive amplification steps according to the manufacturer's recommendations. Two replicates of each experiment were carried out using different microarray slides where the RNA samples from two different sources were labelled with either Cy3- or Cy5-conjugated

deoxyribonucleotides. The fluorescent dye on probes derived from the experimental aRNA was Cy5, while the dye on control probes was Cy3.

cDNA microarrays

We used a commercially available cDNA microarray, the AceGene-Mouse Oligo Chip 30K 1 Chip Version, which contained 30,000 cDNA named human genes, to identify genes altered in the heart and kidney either between TG and WT mice or high salt intake. Labeled probes were mixed with a hybridization solution (5×sodium chloride and sodium citrate (SSC), 0.5% sodium dodecyl sulfate (SDS), 4×Denhardt's solution, 20% hybridization solution, 0.1 mg/ml denatured salmon sperm DNA and 10% Formamide). After hybridization for 14 h at 46 °C, the slides were washed in 5×SSC and 0.1% SDS for 2 min at room temperature, 5×SSC and 0.1% SDS for 10 min at 30 °C, 0.5×SSC for 2 min at room temperature. Slides were scanned for Cy3 and Cy5 fluorescence with a 428 ARRAY scanner (AFFYMETRIX), and the fluorescence was quantified with DNASIS Array software version 2.6 (Hitachi Software Engineering Co., Ltd. Kanagawa, Japan). The current analysis used intensity dependent Global Normalization (Mean: 10,000). Intensity dependent normalization is just one technique used to eliminate dye-related artifacts in two-color experiments such as this. The results for each gene were reported as an average obtained from 3 slides. The data are reported

as the normalized ratio of Cy5 (for coupling factor 6 +) to Cy3 (for coupling factor 6 -). We used intensity of 2,000 or above.

Measurement of intracellular free calcium

The cells were subcultured in 6-cm petri dishes, and were transfected with or without NM_026333. After loading with 5 μmol/L fura-2–AM, intracellular free calcium was measured at excitation wavelengths of 340 and 380 nm and emission wavelength of 510 nm as described previously. Calibration was made using ionomycin followed by EGTA-Tris.

Immunofluorescent staining for autophagy

TG and WT cells were plated at 5×10^5 cells/ml on glass coverslips and allowed to adhere overnight in DMEM containing 10% FBS. In some TG cells, the transfection of DNA was carried out using Lipofectamine 3000 Transfection Kit, according to the manufactures' protocol. Cells were incubated at 4°C for 1 hour in PBS, pH 7.0, containing 1% BSA with either rabbit polyclonal antiserum raised against Lamp 1 or rabbit polyclonal antiserum raised against LC3. Cells were washed and incubated at 4°C for 1 hour in the dark with PBS containing secondary antibody conjugated with Alexa Fluor 488 and 568, both were diluted 1:1000 for 1 hour at room temperature and then rinsed with PBS. Fluorescent images were captured with the use of fluorescence

microscope (BZ-X710; Keyence, Osaka, Japan).

Synthesis of recombinant NM_026333 protein

Recombinant NM_026333 protein was obtained from *Escherichia coli* using a cleavable fusion protein strategy. A cDNA fragment encoding NM_026333 was cleaved from expression vector for NM_026333 cDNA by BamH I and PstI. pGEX-4T-3 was digested XhoI to linearize the vector, and then it was ligated with annealing cassette of PstI site which was created by oligomer pGEX-4T-3 M3 F: 5'-TCGAGTCGACCTGCAGGCATC -3' and oligomer pGEX-4T-3 M3 R: 5'-TCGAGATGCCTGCAGGTCGAC -3'. To obtain recombinant NM_026333 protein, cDNA corresponding to NM_026333 was subcloned into pTrcHisA.

Determination of protein expression

Tissue and cell samples were homogenized in RIPA lysis buffer (20 mmol/l Tris-HCl pH 7.5, 150 mmol/l NaCl, 1 mmol/l EDTA, 1 mmol/l EGTA, 1% Triton X-100, 1% glycerol, 1 mmol/l dithiothreitol and 0.5 mmol/l phenylmethylsulfonyl fluoride). Samples were mixed with Laemelli buffer that contained 5% β-mercaptoethanol and were loaded onto SDS-polyacrylamide gel electrophoresis. Protein was transferred electrophoretically to a polyvinilidene difluoride membrane, and was incubated with the primary antibodies for LC3II, p62, Atg7, HHAC1-4, pan-acetyl H3, pan-acetyl H4,

H4K5, H4K8, H4K12, H3K4me3, H3K9me3, H3K27me3, H4K20me3, NCX1, TRPC3 and 6, Cav1.2, emerin, lamin A/C, HP1α, HMGB1, BAF, and GAPDH at 4°C overnight. The protein bands were detected by the enhanced chemiluminescence plus detection systems. Densitometric analysis was performed with Scion image software, and the relative ratio to the protein bands was calculated in each sample. The band detection was all within the linear range.

Chromatin Immunoprecipitation assay (ChIP)

ChIP assays were performed using C2C12 cells or heart-derived fibroblasts subjected to CF6 at 10^{-7}M for 9 hours. In brief, $5x10^6$ cells were fixed with 1% paraformaldehyde for 5 min and crosslinked; the crosslinked chromatin was then sheared by sonication. The chromatin solution was incubated with 5μg of anti-H4K5 and anti-HDAC3 antibodies or control IgG, and protein A/G plus-agarose immunoprecipitation reagent overnight at 4°C. Immunoprecipitates were eluted from the protein A/G plus-agarose reagent, and supernatants were treated with Rnase A and proteinase K, extracted, and precipitated. The pellets were then resuspended in 30 μl of H_2O, and subjected to 40 cycles of PCR amplification with the following primers specific for the mouse Atg7 promoters.

Luciferase assay

HEK-293 cells were transfected with Atg7 promoter/reporter vectors containing or lacking repressor binding element. The 5′-flanking regions of the Atg7 promoter (+1 to -800, +1 to -400, and +1 to -200) were synthesized (Takara, Japan) and subcloned into the luciferase reporter vector (Picagene basic vector). The pcDNAI/Neo-β-galactosidase plasmid was also cotransfected to monitor the transfection efficiency. The transfected cells were incubated at 37 °C for 24 hours, and then exposed to CF6 at 10^{-7}M for 3 h. The cells were harvested, and cell lysates were assayed with Picagene Luciferase Assay System and Galacto-Light Plus System for the detection of β-galactosidase, as recommended by the manufacturer's instructions. The luciferase activity was normalized with that of β-galactosidase.

Purification of His-tagged protein

TALON magnetic beads (Cat. Nos. 635636 & 635637) was used for microscale purification of his-tagged proteins on a magnetic separator. Tractor buffer was added to cell pellet, and mixed gently by pipetting up and down several times. The sample was centrifuged at 10,000–12,000 x g for 20 min at 4°C to remove any insoluble material, and then the supernatant was carefully transferred to a clean tube without disturbing the pellet. A small portion of this clarified sample was set aside on ice for SDS-PAGE analysis and was proceeded with the TALON magnetic beads purification protocol.

Aliquot of beads was added into a microfuge tube, and was washed with deionized water after removal of storage buffer. After the beads were equilibrated with Equilibration/Wash buffer, the cell lysate was added to the beads and mixed on a rotary shaker for 30 min at room temperature. The beads were washed with Equilibration/Wash buffer three times and the first, second, and third washes were collected, respectively. To elute the protein, Elution buffer was added to bead suspension and mixed for 5 min, and eluate was collected for the following Western blot analysis.

β-gal staining

Senescence-associated β-gal activity was examined as follows. The cells were fixed in a 4% paraformaldehyde solution (pH 7.5) for 15 min and permeabilized with 0.1% Triton X-100 for 15 min at room temperature. The samples were incubated for 24 hours at 37°C in freshly prepared β-gal staining solutions containing 1 mg/mL 5-bromo-4-chrolo-3-indlyl β-D-galactopylanoside (X-gal), 5 mmol/L potassium ferrocyanide, 5 mmol/L potassium fericyanide, 150 mmol/L NaCl, 2 mmol/L $MgCl_2$, 0.01% sodium deoxycholate, and 0.02% Nonidet-40. Then, the stained cells were photographed.

Statistical analysis and ethical considerations

Results were expressed as mean±SEM. Differences between groups were examined for statistical significance using Student's *t* test after Kolmogorov-Smirnov Test or analysis of variance (ANOVA) with Bonferroni's test.

RESULTS

Identification of a key molecule for proton-induced accelerated aging

We recently reported that both CF6-overexpressing TG and high salt-fed mice which had sustained intracellular acidosis, due to enhanced proton import through ecto-F_1F_o complex and/or reduced proton export through Na^+-K^+ ATPase inhibition, displayed shortened lifespan and early senescence-associated phenotypes such as signs of hair greying and alopecia, weight loss, and/or reduced organ mass (9). Mice were fed a normal salt diet until the age of 11 weeks, and were followed by a high salt diet (8% salt; Oriental Yeast, Japan) or by a normal salt diet continuously.

CF6 stimulated proton import by forcing the backward rotation of F_o (10), and inhibited three proton extruders, Na^+-H^+ exchanger, Na^+-HCO_3^- cotransporter, and Na^+-dependent Cl^--HCO_3^- exchanger by decreasing the inwardly directed electrochemical Na^+ gradient which is created by Na^+-K^+-ATPase pump. CF6 and ouabain phosphorylated α subunit of Na^+-K^+-ATPase at serine 943 which was reported

to result in the suppression of its activity (22) and inhibited its activity in cultured fibroblasts. ^{31}P-MRS demonstrated that TG liver displayed the decrease in intracellular pH ranging from 0.1 to 0.15 units compared with WT mice (17), and the pH value of the liver was similar between middle-aged TG and high salt-fed mice.

Up to 75 weeks of age, TG mice appeared morphologically identical to their WT littermates under normal diet; however, at the age of 100 weeks, most of the TG mice manifested the early aging-related phenotype such as signs of hair greying and alopecia, weight loss, and reduced organ mass. The hair in the older TG mice was sparser than that of their WT counterparts, and hair greying was more frequent in TG mice than in WT mice. Like TG mice, high salt-fed mice showed hair greying and alopecia compared with normal salt-fed WT mice. Consistent with accelerated aging, TG and high salt-fed mice were short-lived compared with WT mice

To characterize a key molecule which accelerates aging and shortens lifespan in TG and high salt-fed mice, we screened causative genes in the heart and kidney of TG mice at the age of 7 weeks and high salt-fed mice for 10 weeks by analyzing heart and kidney microarrays. Out of a number of genes, uncharacterized NM_026333 was constantly downregulated in both organs obtained from both types of mice (Table 1, NM_026333n others section). To confirm that accelerated aging is secondary to

downregulation of NM_026333 in both types of mice, we expressed NM_026333 coding 269 amino acids in TG cells which display aging hallmarks of defective proteostasis, histone modification, and genomic instability. We also confirmed a positive β-Gal staining in the ageing phenotype of TG cells (Figure 1a). It is of importance that induction of NM_026333 cancelled expression of whole aging hallmarks such as defective proteostasis, histone modification, and genomic instability in TG cells.

In details, as shown in Figure 1a, LC3 II and lysosome were weakly stained in the peripheral cytoplasm in TG cells compared with a potent peri-nuclear staining in WT cells. In contrast, nuclear LC3 II and lysosome were strongly stained in TG cells despite no staining in WT cells. LC3 II and lysosome completely merged in WT cells but partially in TG cells, showing impaired formation of autolysosome under chronic intracellular acidosis (left panel). The number of autolysosome was decreased in TG cells compared with WT cells, and was recovered in TG cells transfected with NM_026333 (left lower column). Expression of autophagosome lysosome fusion-related molecules (23) such as Rab7, PI4KIIα, and CTTN (cortactin) were downregulated in TG or high salt-fed mice despite no change in other fusion-related genes such as FYCO1, GABARAP, and INPP5E (Table 1). The higher expression of LC3 II and P62 in total cell lysate was observed in TG cells and treatment with

chloroquine at 20 μM did not affect, indicating that chronic impaired autophagy is present in TG cells (right panel). Nuclear acetylated LC3 II was increased in TG cells compared with WT cells, which is consistent with evidence that acetylation suppresses cytoplasmic translocation of LC3 II (24). As shown in Figure 1a, induction of NM_026333 recovered a potent peri-nuclear staining in LC3 II and lysosome, and autolysosome formation in TG cells. As to mitophagy, numerous mitophagy adaptors have been identified so far, including optineurin (OPTN), BRCA1 gene 1 (NBR1), nuclear domain 10 protein 52 (NDP52), and TAX1 binding protein 1 (TAX1BP1). Mitophagy receptors have been identified, including BCL2 interacting protein 3 (BNIP3), Nip3-like protein X (NIX), the FUN14 domain-containing protein 1 (FUNDC1), and cardiolipin and prohibitin 2 (PHB2). Cells lacking these adaptors or receptors fail to induce mitophagy (25). In our mouse models, the expression of NDP52, TBK1, and FUNDC1 was decreased in some organs (Table 1).

By the screening of proteostasis-related compounds, a number of Atgs were coordinately decreased in the heart and kidney of TG or high salt-fed mice. It is noteworthy that Atg7 was commonly decreased in both organs of both kinds of mice, suggesting that Atg7 is one molecule targeted at acidosis-induced defective proteostasis.

In TG cells, Atg7 was decreased compared with that in WT cells like CF6-treated

WT cells (Figure 1b). Treatment of WT cells with ouabain at 10^{-6}M decreased Atg7 concomitantly with increased LC3 II and P62 (Figure 1c). Due to impaired autophagy, tissue fibrosis was greater in TG and high salt-fed mice compared with WT (Figure 1d). Overall, it is characteristics that proton-induced chronic impaired autophagy is due to the decrease in Atg7, impaired formation of autolysosome, and the increase in nuclear acetylated LC3 II. In addition, acetylation of Atg7 might further impaire autophagy. Induction of NM_026333 induced the decrease in LC3 II and P62 and the increase in Atg7.

NM_026333 expressed in various organs such as intestine, duodenum, brain, colon, bladder, liver, placenta, cerebellum, limb, mammary gland, testis, heart, and kidney ubiquitously (26). In TG mice, CF6 was overexpressed in various organs except for adipose tissue (17). Therefore, most organs and cells are vulnerable to ageing insult by proton induction.

Proton-induced epigenetic alterations and genomic instability and impact of NM_026333 on them

We examined impact of sustained intracellular acidosis on aging epigenetic markers such as global hypo-methylated DNA, increased H4K16ac, H4K20me3, or H3K4me3 as well as decreased H3K9me3 or H3K27me3 (1). These markers transmit

as epigenetic memory, and demethylation of H3K4me3 extends lifespan in nematodes (27). As shown in Figure 2a, CF6 increased H3K4me3 and H4K20me3 and decreased H3K9me3 and H3K27me3 in HEK-293 cells. In regard to acetylation, we found a novel aging marker of increased H4K5ac. HDAC3 deacetylates histone lysine residues globally and H4K5 and K12 more rapidly, suggesting the dominant acetylation of H4K5. As shown in Figure 2b, treatment with CF6 at 10^{-7}M or ouabain at 10^{-6}M induced translocation of nuclear HDAC3 to the cytoplasm in WT cells, being concomitant with the same translocation of HDAC4 that is a scaffold for recruiting HDAC3. Furthermore, nuclear emerin, an activator for HDAC3, was decreased in CF6- or ouabain-treated WT or TG cells. Recombinant NM_026333 protein attenuated CF6-dependent translocation of HDAC 3 and 4 in TG cells. Taken together, it is likely that suppression of nuclear HDAC3-HDAC4-emerin system is attributable to H4K5ac formation under chronic intracellular acidosis. As shown in Figure 2c, immunofluorescence analysis confirmed the distinct distribution of HDAC3 that is present only in the nucleus in WT cells, but both in the cytoplasm and nucleus in TG cells.

As to chromosomal stability, we examined the role of sustained intracellular acidosis in nuclear architecture and chromatin remodeling in TG cells.

Heterochromatin assembly at pericentric regions requires trimethylation of histones H3K9 and H4K20, as well as HP1α binding, and is important for chromosomal stability (28). As shown in Figure 2d, CF6 decreased lamin A/C, emerin, and HP1α without affecting BAF and HMGB1 in WT cells like TG cells. This effect led to chromatin remodeling of heterochromatin loss (Figure 2e). Defects in the nuclear architecture, known as laminopathies, can cause genome instability and result in premature aging syndromes, in addition to direct lesions of exogenous agents and endogenous threats in the DNA. Genetic variants of lamin A/C, progerin, reduces the transcription of antioxidant genes and promotes genomic instability (1).

Induction of NM_026333 rescued TG cells from genomic instability by the increase in lamin A/C, emerin, and HP1α (Figure 1a), and epigenetic alterations by normalizing the increase in H3K4me3 and H4K20 me3, the decrease in H3K9me3 and H3K27me3, and the increase in H4K5ac (Figure 2f) and by restoration of heterochromatin (Figure 2g).

NCX1 is a target molecule of NM_026333 and implications in aging mechanisms

To gain insight into the anti-aging mechanism for NM_026333, we characterized subcellular localization of NM_026333 coding 269 amino acids in HEK-293 cells. NM_026333 protein was translocated into the plasma membrane in HEK-293 cells

(Figure 3a), which is consistent with the presence of the trans-membranous neuregulin region (90-193aa). We searched a target molecule of NM_026333 to gain insight into the mechanism underlying proton-induced aging. Because NM_026333 was translocated in the plasma membrane, we focused on membrane proteins such as ion channels as the target of NM_026333 using immunoprecipitation study of TALON magnetic beads. In His-tagged NM_026333-transfected HEK-293 cells, plasma membrane channel, Na^{+}-Ca^{2+} exchanger 1 (NCX1) was detected by protein-protein interaction after microscale purification of His-tagged proteins with TALON magnetic beads (Figure 3b). Other channels such as TRPC3, TRPC6, and Cav 1.2 were not detected. NM_026333 attenuated acetylcholine-induced Ca^{2+} influx (Figures 3c), indicating that NM-026333 interacted with NCX1 to suppress its reverse mode.

We further examined the role of NCX1 in the proton-induced aging mechanism. Treatment with SN-6, a selective inhibitor for NCX1, at 10^{-5}M rescued TG cells from expression of aging hallmarks such as genomic instability (Figure 3d), impaired autophagy (Figure 3d), histone modification (Figure 3d), and chromatin remodeling (Figure 3e). Importantly, SN-6 at 10^{-5}M rescued human cells, HEK-293 cells treated with CF6, from expression of aging hallmarks of genomic instability (Figure 3f), impaired autophagy (Figure 3f), and histone modification (Figure 3f) with

suppression of Ca^{2+} influx (Figure 3g). SN-6 at 10^{-5}M attenuated CF6-dependent translocation of HDAC3 and 4 in TG cells (Figure 2b). Overall, these suggest that NCX1, which is present at the downstream of NM_026333, plays an important role in CF6-induced, proton-mediated accelerated aging.

Interaction between epigenetic alterations and impaired autophagy

We examined whether H3K4me3, H4K20me3, H3K9me3, H3K27me3, and H4K5ac contribute to the decrease in Atg7 expression. We analyzed the mouse Atg7 promoter at -1 through -1000 (the transcription starting site) by TFsearch, and found a number of repressor binding sites consisting of Cdx A, GATA-2, and SRY between -441 and -763 (Figure 4a). Indeed, deletion of this repressive region at -800 through -400 resulted in an increase in luciferase activity in response to CF6 at 10^{-7}M (Figure 4b). ChIP assay revealed that H4K5ac, H3K4me3, and H4K20me3 at the region between -441 through -763 were increased in TG cells compared with WT cells, and were enhanced by CF6 and ouabain in C2C12 mouse-derived skeletal muscle cells (Figures 4c and 4d). Either recombinant NM_026333 protein or SN-6 at 10^{-5}M cancelled CF6-induced increase in H4K5ac H3K4me3, and H4K20me3 at the region between -441 through -763 in C2C12 cells. Conversely, HDAC3, pan-acetyl H3, H4K8ac, and H4K12ac at the region between -441 through -763 were decreased or unchanged by

CF6 (Figure 4c). In other promoter regions, neither CF6 nor ouabain affected pan-acetyl histone H3, H4K5, H4K8, or K12 in C2C12 cells (Figure 4e). Collectively, CF6-induced H4K5ac, H3K4me3, and H4K20me3 are attributable to the decrease in Atg7 in TG and high salt-fed mice. Induction of NM_026333 to C2C12 cells cancelled CF6-induced increase in H4K5ac, H3K4me3, and H4K20me3 at the region between -441 through -763. As to downregulated histone trimethylation, H3K9me3and H3K27me3 at the region between -441 through -763 were enhanced by CF6 and ouabain in C2C12 mouse-derived skeletal muscle cells (Figure 4f).

Impact of recombinant NM_026333 protein on proton-induced epigenetic alterations and genomic instability

As shown in Figure 5a, an expression protein by transfecting NM_026333 to HEK-293 cells showed expected molecular weight at 30 kD. Incubation of His-tagged recombinant NM_026333 protein with lysate of TG and HEK293 cells confirmed again NCX1 as a protein-protein interaction target for NM_026333 using TALON magnetic beads for purification of His-tagged proteins (Figure 5b). Recombinant NM_026333 protein at 10^{-4}M rescued TG cells from genomic instability by the increase in emerin, and HP1α, impaired autophagy by the increase in Atg7 and the decrease in LC3II, and epigenetic alterations by the decrease in H3K4me3 in 48 hours (Figure 5c). Treatment

with recombinant protein also rescued human cells, HEK-293 cells treated with CF6, from expression of aging hallmarks of genomic instability, impaired autophagy, and histone modification (Figure 5c) with suppression of Ca^{2+} influx (Figure 5d).

Impact of NCX1 in lifespan in TG mice

To further investigate *in vivo* role of NCX1 in lifespan, we examined whether intraperitoneal injection of SN-6 may extend lifespan in old-aged TG mice (n=20). We administered SN-6 at 3 mg/kg or vehicle by intraperitoneal injection to 100-week-old TG mice on every other day. Compared with vehicle-treatment, SN-6 extended four weeks in lifespan (median values; 118±2 vs 122±2 weeks, $p<0.05$) without affecting daily activity. The single dose of SN-6 at 3 mg/kg is relevant to the dose which reduced the cerebral infarct volume in mice when administered at 30 minutes before 4-hour occlusion of the middle cerebral artery followed by 24 hours of reperfusion.

DISCUSSION

The major findings of this study were as follows. We discovered NM_026333 as anti-aging gene which was commonly downregulated in the heart and kidney in sustained intracellular acidosis mice. Induction of novel anti-aging gene, NM_026333,

or recombinant protein rescued TG cells from impaired autophagy, genomic instability, and epigenetic alteration. NM_026333 protein bound NCX1 to suppress its reverse mode, and inhibition of NCX1 rescued human cells as well as TG cells from whole aging hallmarks.

NM_026333 as novel anti-aging gene against proton-induced accelerated aging

To gain insight into the aging pathway, we searched its causative genes in the heart and kidney in both TG and high salt-fed mice. NM_026333 was commonly downregulated in both organs obtained from both types of mice, and induction of NM_026333 in TG cells canceled expression of whole aging hallmarks such as impaired autophagy, genomic instability, and histone modification, suggesting that NM_026333 is a novel anti-aging gene.

NM_026333 contributed to the decrease in Atg7 via epigenetic alterations. Atg7 is a key E1 like enzyme for two conjugation modifiers, Atg12 and LC, and is associated with p53-mediated cell division and apoptosis (29). The Atg12–Atg5–Atg16L1 complex is required for formation of the covalent bond between LC3 and phosphatidylethanolamine (LC3 II), and plays an important role in the elongation and closure of the isolation membrane with LC3 II. Importance of Atg7 for aging has been displayed by evidence that its knockdown abolishes lifespan extension due to daf-2 loss,

dietary restriction, or rapamycin, and accelerates the aging-related phenotype by ubiquitinylated protein aggregates, peroxisomes, and mitochondria (30). Furthermore, loss of autophagy induced by Atg7 knockdown leads to decreased levels of checkpoint kinase 1 (Chk1) and a greatly diminished ability to repair DNA double-strand breaks by homologous recombination (31).

In regard to anti-aging gene, genome-wide association studies identified loci consistently associated with longevity were only APOE, FOXO3 and 5q33.3 (32) despite the fact that thousands of single-nucleotide polymorphisms are associated with common human diseases and traits (33). In the present study, we found a novel anti-aging gene, NM_026333, in proton-induced accelerated aging mouse models. It is intriguing that NM_026333 binds and suppresses NCX1 by protein-protein interaction, and SN-6, a selective inhibitor for NCX1 and a mimic effector of NM_026333, rescued human cells as well as TG cells from expression of whole aging hallmarks like induction of NM_026333. In regard to association of ion channel with aging, voltage-gated calcium channel UNC-36 (CACNA2D2) and SLC7A6 (cationic amino acid transporter) were shown to be involved in longevity in C. elegans (34). However, Unc-36 is known to have reduced pharyngeal pumping, limiting food intake and resulting in a genetic mimetic of diet restriction similar to eat-2 mutation. Zhang et al.

(35) identified a thermosensitive TRP channel as a mediator of longevity, but it was limited in the critical life stages during which temperature influences. In the present study, we discovered NM_026333 as a novel anti-aging gene, and its target molecule was NCX1.

NCX1 as a target for novel anti-aging therapy

Mammalian NCX forms a multigene family comprising NCX1, NCX2, and NCX3. NM_026333-targeted NCX1 is highly expressed in the heart, kidney, and brain and at much lower levels in other tissues, whereas the expression of NCX2 and NCX3 is limited mainly to the brain and skeletal muscle (36). The NCX1 is a plasma membrane channel protein that maintains intracellular Ca^{2+} balance and allows for proper relaxation under different physiological conditions. Not only supplement of NM_026333 but also inhibition of NCX1, a protein-protein interaction target of NM_026333, prevented whole accelerated aging signals, providing important implications in novel anti-aging therapy. NCX1 can either extrude Ca^{2+} from the cytosol in exchange for Na^{+} as a forward mode or vice versa (Ca^{2+} in and Na^{+} out) as a reverse mode (36). However, it works in a reverse mode in most of the pathological conditions, including arrhythmia, myocardial necrosis, contractile failure, diabetes, and cancer (36-38). Therefore, blockade for the reverse mode of NCX1 may be beneficial. Even in

anti-aging therapy, it is convenient because activation of the reverse mode of NCX1, which is due to down-regulation of NM_026333, accelerates aging.

Blockade of NCX1 with a selective inhibitor SN-6 enhances NO-mediated relaxation (39). The reverse-mode NCX1 activity inhibitor KB-R7943 promotes prostate cancer cell death by activating the JNK pathway and blocking autophagic flux (40). Downregulation of NCX1 leads to an increase in β-cell function, proliferation, mass, and resistance to physiologic stress, namely to various changes in β-cell function that are opposite to the major abnormalities seen in type 2 diabetes (41). All shows that inhibition of the reverse mode of NCX1 may be beneficial in vasculature, glucose metabolism, and cancer therapy, suggesting one possibility of its clinical usage for anti-aging. It was reported that KB-R7943, SN-6, and SEA0400 inhibited preferentially the unidirectional outward NCX1 (Ca^{2+} influx reverse mode) rather than the unidirectional NCX1 (Ca^{2+} efflux forward mode) in isolated guinea pig cardiac ventricular cells (42). Thus, instead of NM_026333, usage of SN-6 might provide evidence for a definite function of NCX1 in aging and possibility of a target molecule for anti-aging therapy.

In conclusion, chronic intracellular acidosis induced by circulating mitochondrial peptide or high salt intake engages in a mutually stimulatory amplification cascade of

aging, being orchestrated by NM_026333-NCX1 axis. The present findings will widen our understanding of aging mechanism, and provide implications in a novel pharmaceutical target for anti-aging therapy.

Study strengths and limitations

We discovered NM_026333 as a novel anti-aging gene [coupling factor 6-related NCX1-mediated anti-aging protein (CNAP) gene] from the heart and kidney of proton-induced aging models. This recombinant protein rescued TG cells and CF6-treated human cells from aging hallmarks. Thus, NM_026333 might be a novel pharmaceutical target for anti-aging therapy. However, there are some limitations in the structural analysis and the long-term effect of this protein on aging phenotype and lifespan. Furthermore, the issues concerning "which cell type in the heart expresses NM_026333", "whether or not NM_026333 goes down in normal aging model", and the impact of SN-6 on cardiac function, cardiac fibrosis and other parameters in heart or autophagy in TG mice remain to be elucidated. The interaction site of this protein with NCX1 may be important to understand the mechanism for proton-induced aging and to search a novel pharmaceutical target.

Author contributions

TO, MT, KI, KM (Koji M), MT, KM (Kasumi M), TT, HT, and KO contributed to designing research studies. TO, MT, KI, and KM (Koji M) contributed to conducting experiments, acquiring data, and analyzing data. TO and KO contributed to providing reagents and writing the manuscript.

Acknowledgement

This work is supported by Grant-in-Aid for Scientific Research (No. 19590800, 21590946, and 15K09151 for TO) from the Ministry of Education, Culture, Sports, Science and Technology, Japan.

Conflict of Interest

None

References

1. López-Otín C, Blasco MA, Partridge L, Serrano M, Kroemer G. 2013. The hallmarks of aging. *Cell*. .153:1194-1217.

2. Mattison JA, Colman RJ, Beasley TM, Allison DB, Kemnitz JW, Roth GS, Ingram DK, Weindruch R, de Cabo R, Anderson RM. 2017. Caloric restriction improves health and survival of rhesus monkeys. *Nat Commun*. 8:14063.

3. Baker DJ, Childs BG, Durik M, Wijers ME, Sieben CJ, Zhong J, Saltness RA, Jeganathan KB, Verzosa GC, Pezeshki A, Khazaie K, Miller JD, van Deursen JM. 2016. Naturally occurring p16(Ink4a)-positive cells shorten healthy lifespan. *Nature*. 530 (7589):184-189.

4. Buclin T, Cosma M, Appenzeller M, Jacquet AF, Décosterd LA, Biollaz J, Burckhardt P. 2001. Diet acids and alkalis influence calcium retention in bone. *Osteoporos Int*. 12:493–499.

5. Fagherazzi G, Vilier A, Bonnet F, Lajous M, Balkau B, Boutron-Rualt MC, Clavel-Chapelon F. 2014. Dietary acid load and risk of type 2 diabetes: The E3N-EPIC cohort study. *Diabetologia* 57:313–320.

6. Murakami K, Sasaki S, Takahashi Y, Uenishi K. 2008. Association between dietary acid-base load and cardiometabolic risk factors in young Japanese women. *Br J Nutr*.

100:642–651.

7. Raphael KL, Murphy RA, Shlipak MG, Satterfield S, Huston HK, Sebastian A, Sellmeyer DE, Patel KV, Newman AB, Sarnak MJ, Ix JH, Fried LF; Health ABC Study. 2016. Bicarbonate Concentration, Acid-Base Status, and Mortality in the Health, Aging, and Body Composition Study. *Clin J Am Soc Nephrol*. 11:308-316.
8. Osanai T, Tanaka M, Mikami K, Kitajima M, Magota K, Tomita H, Okumura K. 2018. Mitochondrial inhibitory factor protein 1 attenuates coupling factor 6-induced aging signal. *J Cell Biochem*. 119:6194-6203.
9. Osanai T, Tanaka M, Izumiyama K, Mikami K, Kitajima M, Tomisawa T, Magota K, Tomita H, Okumura K. Intracellular protons accelerate aging and switch on aging hallmarks in mice. 2018. *J Cell Biochem* in press.
10. Osanai T, Magota K, Tanaka M, Shimada M, Murakami R, Sasaki S, Tomita H, Maeda N, Okumura K. 2005. Intracellular signaling for vasoconstrictor coupling factor 6: novel function of β-subunit of ATP synthase as receptor. *Hypertension*. 46:1140-1146.
11. Osanai T, Kamada T, Fujiwara N, Katoh T, Takahashi K, Kimura M, Satoh K, Magota K, Kodama S, Tanaka T, Okumura K. 1998. A novel inhibitory effect on prostacyclin synthesis of coupling factor 6 extracted from the heart of spontaneously

hypertensive rats. *J Biol Chem*. 273:31778-31783.

12. Tanaka M, Osanai T, Murakami R, Sasaki S, Tomita H, Maeda N, Satoh K, Magota K, Okumura K. 2006. Effect of vasoconstrictor coupling factor 6 on gene expression profile in human vascular endothelial cells: enhanced release of asymmetric dimethylarginine. *J Hypertens*. 24:489-497.
13. Kumagai A, Osanai T, Katoh C, Tanaka M, Tomita H, Morimoto T, Murakami R, Magota K, Okumura K. 2008. Coupling factor 6 downregulates platelet endothelial cell adhesion molecule-1 via c-Src activation and acts as a proatherogenic molecule. *Atherosclerosis*. 200:45-50.
14. Osanai T, Tanaka M, Kamada T, Nakano T, Takahashi K, Okada S, Sirato K, Magota K, Kodama S, Okumura K. 2001. Mitochondrial coupling factor 6 as a novel endogenous vasoconstrictor. *J Clin Invest*. 108:1023-1030.
15. Osanai T, Tomita H, Kushibiki M, Yamada M, Tanaka M, Ashitate T, Echizen T, Katoh C, Magota K, Okumura K. 2009. Coupling factor 6 enhances Src-mediated responsiveness to angiotensin II in resistance arterioles and cells. *Cardiovasc Res*. 81:780-787
16. Izumiyama K, Osanai T, Sagara S, Yamamoto Y, Itoh T, Sukekawa T, Nishizaki F, Magota K, Okumura K. 2012. Estrogen attenuates coupling factor 6-induced

salt-sensitive hypertension and cardiac systolic dysfunction in mice. *Hypertens Res*. 35:539-546.

17. Osanai T, Tanaka M, Magota K, Tomita H, Okumura K. 2012. Coupling factor 6-induced activation of ecto-F1Fo complex induces insulin resistance, mild glucose intolerance and elevated blood pressure in mice. *Diabetologia*. 55:520-529.
18. Osanai T, Nakamura M, Sasaki S, Tomita H, Saitoh M, Osawa H, Yamabe H, Murakami S, Magota K, Okumura K. 2003. Plasma concentration of coupling factor 6 and cardiovascular events in patients with end-stage renal disease. *Kidney Int*. 64:2291-2297.
19. Osanai T, Sasaki S, Kamada T, Fujiwara N, Nakano T, Tomita H, Matsunaga T, Magota K, Okumura K. 2003. Circulating coupling factor 6 in human hypertension: role of reactive oxygen species. *J Hypertens*. 21:2323-2328.
20. Osanai T, Fujiwara N, Sasaki S, Metoki N, Saitoh G, Tomita H, Nishimura T, Shibitani S, Yokoyama H, Konta Y, Magota K, Okumura K. 2010. Novel pro-atherogenic molecule coupling factor 6 is elevated in patients with stroke: A possible linkage to homocysteine. *Ann Med*. 42:79-86.
21. Li XL, Xing QC, Gao YY, Dong B, Pang YZ, Jiang HF, Tang CS. 2007. Plasma level of mitochondrial coupling factor 6 increases in patients with type 2 diabetes

mellitus. *Int J Cardiol*. 117:411-412.

22. Cheng XJ, Fisone G, Aizman O, Aizman R, Levenson R, Greengard P, Aperia A. 1997. PKA-mediated phosphorylation and inhibition of Na(+)-K(+)-ATPase in response to beta-adrenergic hormone. *Am J Physiol*. 273:C893-901.
23. Martens S, Nakamura S, Yoshimori T. 2016. Phospholipids in autophagosome formation and fusion. *J Mol Biol*. 428:4819-4827.
24. Huang R, Xu Y, Wan W, Shou X, Qian J, You Z, Liu B, Chang C, Zhou T, Lippincott-Schwartz J, Liu W. 2015. Deacetylation of nuclear LC3 drives autophagy initiation under starvation. *Mol Cell*. 57:456-466.
25. Gkikas I, Palikaras K, Tavernarakis N. 2018. The Role of Mitophagy in Innate Immunity. *Front Immunol*. 9:1283. doi: 10.3389/fimmu.2018.01283.
26. Mouse ENCODE Consortium. 2014. A comparative encyclopedia of DNA elements in the mouse genome. *Nature*. 515:355-364.
27. Greer EL, Maures TJ, Hauswirth AG, Green EM, Leeman DS, Maro GS, Han S, Banko MR, Gozani O, Brunet A. 2010. Members of the H3K4 trimethylation complex regulate lifespan in a germline-dependent manner in C. elegans. *Nature*. 466:383-387.
28. Schotta G, Lachner M, Sarma K, Ebert A, Sengupta R, Reuter G, Reinberg D,

Jenuwein T. 2004. A silencing pathway to induce H3-K9 and H4-K20 trimethylation at constitutive heterochromatin. *Genes Dev*. 18:1251–1262.

29. Lee IH, Kawai Y, Fergusson MM, Rovira II, Bishop AJ, Motoyama N, Cao L, Finkel T. 2012. Atg7 modulates p53 activity to regulate cell cycle and survival during metabolic stress. *Science*. 336:225-228.

30. Rubinsztein DC, Mariño G, Kroemer G. 2011. Autophagy and aging. *Cell*. 146:682-695.

31. Liu EY, Xu N, O'Prey J, Lao LY, Joshi S, Long JS, O'Prey M, Croft DR, Beaumatin F, Baudot AD, Mrschtik M, Rosenfeldt M, Zhang Y, Gillespie DA, Ryana KM. 2015. Loss of autophagy causes a synthetic lethal deficiency in DNA repair. *Proc Natl Acad Sci USA*. 112:773-778

32. Broer L, Buchman AS, Deelen J, Evans DS, Faul JD, Lunetta KL, Sebastiani P, Smith JA, Smith AV, Tanaka T, Yu L, Arnold AM, Aspelund T, Benjamin EJ, De Jager PL, Eirkisdottir G, Evans DA, Garcia ME, Hofman A, Kaplan RC, Kardia SL, Kiel DP, Oostra BA, Orwoll ES, Parimi N, Psaty BM, Rivadeneira F, Rotter JI, Seshadri S, Singleton A, Tiemeier H, Uitterlinden AG, Zhao W, Bandinelli S, Bennett DA, Ferrucci L, Gudnason V, Harris TB, Karasik D, Launer LJ, Perls TT, Slagboom PE, Tranah GJ, Weir DR, Newman AB, van Duijn CM, Murabito JM.

2014. GWAS of longevity in CHARGE consortium confirms APOE and FOXO3 candidacy. *J. Gerontol. A Biol. Sci. Med. Sci*. 70:110–118..

33. Eicher JD, Landowski C, Stackhouse B, Sloan A, Chen W, Jensen N, Lien JP, Leslie R, Johnson AD. 2014. GRASP v2.0: an update on the Genome-Wide Repository of Associations between SNPs and phenotypes. *Nucleic Acids Res*. 43:D799–D804.

34. Sutphin GL, Backer G, Sheehan S, Bean S, Corban C, Liu T, Peters MJ, van Meurs JBJ, Murabito JM, Johnson AD, Korstanje R; Cohorts for Heart and Aging Research in Genomic Epidemiology (CHARGE) Consortium Gene Expression Working Group. 2017. Caenorhabditis elegans orthologs of human genes differentially expressed with age are enriched for determinants of longevity. *Aging Cell*. 16:672-682.

35. Zhang B, Xiao R, Ronan EA, He Y, Hsu AL, Liu J, Xu XZ. 2015. Environmental temperature differentially modulates Caenorhabditis elegans longevity through a thermosensitive TRP channel. *Cell Rep*. 11:1414-1424.

36. Lytton J. 2007. Na^+/Ca^{2+} exchangers: three mammalian gene families control Ca^{2+} transport. *Biochem J*. 406:365-382.

37. Antoons G, Willems R, Sipido KR. 2012. Alternative strategies in arrhythmia

therapy: evaluation of Na/Ca exchange as an anti-arrhythmic target. *Pharmacol Ther*. 134:26-42.

38. Svensson KJ, Kucharzewska P, Christianson HC, Skold S, Lofstedt T, Johansson MC, Morgelin M, Bengzon J, Ruf W, Belting M. 2011. Hypoxia triggers a proangiogenic pathway involving cancer cell microvesicles and PAR-2-mediated heparin-binding EGF signaling in endothelial cells. *Proc Natl Acad Sci USA*. 108:13147-13152.

39. Nishiyama K, Azuma YT, Kita S, Azuma N, Hayashi S, Nakajima H, Iwamoto T, Takeuchi T. 2013. Na^+/Ca^{2+} exchanger 1/2 double-heterozygote knockout mice display increased nitric oxide component and altered colonic motility. *J Pharmacol Sci*. 123:235-45.

40. Long Z, Chen B, Liu Q, Zhao J, Yang Z, Dong X, Xia L, Huang S, Hu X, Song B, Li L. 2016. The reverse-mode NCX1 activity inhibitor KB-R7943 promotes prostate cancer cell death by activating the JNK pathway and blocking autophagic flux. *Oncotarget*. 7:42059-42070.

41. Nguidjoe E, Sokolow S, Bigabwa S, Pachera N, D'Amico E, Allagnat F, Vanderwinden JM, Sener A, Manto M, Depreter M, Mast J, Joanny G, Montanya E, Rahier J, Cardozo AK, Eizirik DL, Schurmans S, Herchuelz A. 2011. Heterozygous

inactivation of the Na/Ca exchanger increases glucose-induced insulin release, β-cell proliferation, and mass. *Diabetes*. 60:2076-2085.

42. Niu CF, Watanabe Y, Ono K, Iwamoto T, Yamashita K, Satoh H, Urushida T, Hayashi H, Kimura J. 2007. Characterization of SN-6, a novel benzyloxyphenyl Na^+/Ca^{2+} exchange inhibitor in guinea pig ventricular myocytes. *Eur J Pharmacol*. 573:161-169.

Table 1. Microarray data of heart and kidney form TG or high salt-fed mice

Gene ID	Gene Name	TG Heart	TG Kidney	Salt Heart	Salt Kidney
UPR,Proteostasis					
NM_012016	IRE-1 (ern2)	0.919±0.024	0.998±0.126	0.944±0.170	0.815±0.129
NM_023913	IRE-1 (ern1)	0.992±0.114	0.862±0.071	0.870±0.069	0.988±0.325
18079	ATF6	0.942±0.202	0.678±0.147	1.471±0.489	1.753±1.632
NM_009716	ATF4	0.993±0.140	1.079±0.332	1.096±0.212	0.810±0.189
AF059275	HSF-1	0.934±0.143	0.957±0.150	1.006±0.165	1.037±0.110
NM_031165	HSC70	0.912±0.206	1.138±0.177	0.829±0.279	0.867±0.393
NM_013863	BAG3	1.042±0.058	0.942±0.630	1.453±0.509	1.320±0.640
NM_019719	CHIP	1.026±0.023	0.914±0.072	1.419±0.220	1.062±0.156
NM_010125	PERK	1.100±0.859	0.660±0.160	0.562±0.108	0.494±0.278
9213	UHRF2	1.010±0.070	1.076±0.062	1.285±0.183	1.227±0.094
8300	SSBP1	0.914±0.022	1.009±0.238	1.317±0.363	0.814±0.389
NM_008884	PML	1.023±0.095	0.796±0.083	0.806±0.195	0.771±0.064
18985	FYCO1	0.867±0.069	0.663±0.451	0.756±0.156	0.958±0.175

NM_009005	Rab7	0.661±0.110	0.866±0.123	0.610±0.279	0.735±0.410
NM_019749	GABARAP	1.126±0.172	1.152±0.140	1.027±0.206	1.064±0.320
17139	PI4KIIα	0.550±0.331	0.720±0.138	0.670±0.260	1.003±0.565
NM_033134	INPP5E	0.917±0.324	1.231±0.335	0.865±0.147	0.879±0.156
NM_007803	CTTN (cortactin)	0.581±0.481	0.622±0.311	0.510±0.313	0.539±0.464
Mitophagy					
10521	OPTN	1.201±0.288	0.925±0.176	1.032±0.170	1.131±0.523
NM_00867	NBR1	1.117±0.124	1.077±0.241	1.120±0.232	0.922±0.275
22059	NDP52	0.979±0.088	0.694±0.306	0.343±0.193	0.423±0.209
29178	NDP52	0.869±0.068	0.779±0.175	0.838±0.229	0.184±0.368
NM_025816	TAX1BP1	0.933±0.071	1.126±0.156	0.952±0.232	0.934±0.178
3872	PINK1	0.801±0.188	0.835±0.267	1.032±0.325	0.952±0.299
NM_019786	TBK1	1.013±0.287	0.754±0.229	1.040±0.330	0.447±0.310
NM_009760	BNIP3	0.826±0.208	0.988±0.096	1.023±0.192	0.905±0.280
25149	FUNDC1	0.739±0.189	0.785±0.114	0.749±0.201	0.855±0.502
NM_007531	PHB2	1.119±0.320	1.028±0.242	1.557±0.165	1.118±0.231
Channels					
NM_011543	TRPC1	0.822±0.128	0.685±0.312	0.805±0.250	0.940±0.317

NM_019510	TRPC3	0.448±0.168	0.583±0.283	0.828±0.311	0.323±0.240
NM_013838	TRPC6	0.957±0.184	1.078±0.077	0.725±0.164	0.932±0.119
NM_012035	TRPC7	1.052±0.252	1.233±0.224	1.117±1.563	0.493±0.119
NM_021450	TRPM7	0.621±0.250	0.695±0.287	0.535±0.155	0.693±0.353
NM_009287	Stim1	0.987±0.112	0.957±0.030	0.638±0.167	0.781±0.174
NM_011406	NCX1 (SLC8A1)	1.007±0.221	0.817±0.180	1.062±0.301	0.903±0.194
Others					
NM_022657	FGF23	0.793±0.132	0.788±0.221	0.604±0.076	0.738±0.379
NM_013823	Klotho	1.154±0.165	0.969±0.070	1.150±0.199	1.084±0.285
NM_010206	FGFR1	1.061±0.065	1.080±0.167	1.442±0.393	1.346±0.176
10788	α-tubulin	0.897±0.333	0.684±0.176	0.000±0.000	0.254±0.317
17242	NPM1	0.974±0.100	1.017±0.204	1.230±0.264	1.211±0.355
NM_00872	NPM1	0.981±0.069	0.889±0.119	1.089±0.295	0.994±0.268
2959	SLC4A7	0.971±0.142	1.087±0.096	1.087±0.103	1.161±0.133
14172	SLC4A7	1.058±0.190	0.987±0.260	1.211±0.500	0.835±0.236
NM_021531	CARM1	1.054±0.089	0.898±0.140	1.102±0.109	0.792±0.308
NM_016694	Parkin	1.048±0.232	0.913±0.138	1.105±0.267	0.779±0.265
NM_007512	ATPIF1	0.819±0.195	0.757±0.103	1.071±0.173	1.114±0.413

NM_026333	uncharacterized	0.375±0.042	0.430±0.209	0.655±0.138	0.204±0.408
NM_009360	TFAM	0.492±0.177	0.665±0.302	1.177±0.318	0.785±0.251

Figure 1. Proton induces accelerated aging through downregulation of anti-aging gene NM_026333

a. Immunofluorescence microscopy of LC3II and LAMP1 (lysosome marker) and proteins of LC3II, nuclear LC3II, nuclear acetylated LC3II, p62, atg7, lamina, lamp1, HP1α, and HMGB1 in TG and WT cells transfected with or without NM_026333 (n=4). β-Gal staining in WT and TG cells * $p<0.05$ vs WT. **b.** Atg7 in WT cells treated with or without CF6 at 10^{-7}M for 24 hours and TG cells (n=3, respectively). * $p<0.05$ vs WT. **c.** Atg7, LC3II, and p62 in TG and WT cells treated with or without CF6 at 10^{-7}M or ouabain at 10^{-6}M for 24 hours (n=4, respectively). * $p<0.05$ vs WT. **d.** Tissue fibrosis in the heart and liver obtained from TG, WT, and high salt-fed WT and TG mice (n=6, respectively). * $p<0.05$ vs normal salt-fed WT.

Figure 2. Epigenetic alterations and genomic instability

a. Epigenetic markers for aging of histone H4K20me3, H3K4me3, H3K9me, and H3K27me3 in HEK 293 cells treated with or without CF6 at 10^{-7}M for 24 hours (n=3).

Representative pictures were shown. **b.** Effect of protons on histone deacetylases (HDACs) expression in TG and WT cells treated with or without CF6 at 10^{-7}M or ouabain at 10^{-7}M (n=3). Effect of recombinant NM_026333 protein and SN-6 on proton-induced HDAC expression in TG and WT cells (n=3). * $p<0.05$ vs WT. **c.** Immunofluorescence analysis for distribution of HDAC3 in WT and TG cells. The distinct distribution of HDAC3 that is present only in the nucleus in WT cells, but both in the cytoplasm and nucleus in TG cells. **d.** Nuclear architecture in WT cells treated with or without CF6 at 10^{-7}M for 24 hours and TG cells (n=3). * $p<0.05$ vs WT (CF6-). **e.** Chromatin remodeling under sustained acidosis in WT cells treated with or without CF6 at 10^{-7}M for 24 hours and TG cells. Representative pictures were shown. Similar results were obtained in separate three experiments. **f.** H4K5ac, H3K4 trimethylation (me3), H4K20me3, H3K9me3, and H3K27me3 in WT and TG cells transfected with or without NM_026333 (n=4). * $p<0.05$ vs WT. **g.** Chromatin structure in TG cells transfected with NM_026333.

Figure 3. Effect of NCX1 inhibition on genomic instability, defective proteostasis, and epigenetic alterations.

a Immunofluorescence microscopy of HEK293 cells transfected with NM_026333. **b.**

Protein-protein interaction after microscale purification of his-tagged NM_026333-transfected HEK-293 cells with TALON magnetic beads. NCX1: Na^+-Ca^{2+} exchanger 1. Representative bands for Western blot were shown. Similar results were obtained in separate experiments. **c.** Acetylcholine-induced Ca^{2+} waveform in HEK293 cells transfected with or without NM_026333 in the presence or absence of extracellular Ca^{2+}. **d.** Effect of SN-6 at 10^{-5}M for 24 hours on primary aging hallmarks of genomic instability (emerin and HP1α), defective proteostasis (LC3II, Atg7, and P62), and epigenetic alterations (H3K9me3 and H3K27me3) in TG cells (n=4). * $p<0.05$ vs WT cells. **e.** Chromatin structure in TG cells treated with SN-6 at 10^{-6}M for 24 hours. **f.** Effect of SN-6 at 10^{-5}M for 24 hours on primary aging hallmarks of genomic instability (emerin and HP1α), defective proteostasis (LC3II, Atg7, and P62), and epigenetic alterations (H3K9me3 and H3K27me3) in HEK 293 cells under 24-hour 10^{-7}M CF6 stimulation (n=4). * $p<0.05$ vs HEK 293 cells. **g.** Effect of SN-6 at 10^{-5}M for 10 minutes on 10^{-6}M acetylcholine-induced Ca^{2+} waveform in HEK293 cells. Representative Ca^{2+} waveforms were shown. Similar results were obtained in separate three experiments.

Figure 4. Atg7 promoter and epigenetic interactions.

a. Mouse Atg7 promoter at -1 through -1000 relative to the transcription start site and binding sites of repressors (Cdx A, GATA-2, and SRY). **b.** Luciferase activity of Atg7 promotor in response to CF6 at 10^{-7}M for 6 hours (n=5). * $p<0.05$. **c.** ChIP assay for H4K5ac, H3K4me3, and H4K20me3 in the Atg7 promoter (primer 4:-440 to -764) in mouse-derived skeletal muscle cell line C2C12. +: treatment with CF6 at 10^{-7} M for 9 hours (left panel) and +: treatment with ouabain at 10^{-6}M for 9 hours (right panel) (n=4, respectively). Treatment with CF6 at 10^{-7}M plus recombinant NM_026333 protein or SN-6 at 10^{-5}M (n=3, lower panel) * $p<0.05$ vs each control. **d.** ChIP assay for interaction between H4K5ac or sirtuin 6 and the Atg7 promoter (primer 4:-440 to -764) in C2C12, WT, and TG cells **e.** ChIP assay for interaction between histone modification and the Atg7 promoter (promer 1:+11 to -291, primer 2:-303 to -406, primer 3: -363 to -478) in mouse-derived skeletal muscle cell line C2C12. +: treatment with coupling factor 6 (CF6) at 10^{-7}M for 9 hours (upper panel) and +: treatment with ouabain at 10^{-6} M for 9 hours (lower panel) (n=3-4). **f.** ChIP assay for interaction between H3K9me3 or H3K27me3 and the Atg7 promoter (primer 4:-440 to -764, primer 3: -363 to -478) in mouse-derived skeletal muscle cell line C2C12; CF6 displays treatment with CF6 at 10^{-7}M for 9 hours, and Ouab displays treatment with ouabain at 10^{-6} M for 9 hours.

Figure 5. Effect of recombinant NM_026333 protein on genomic instability, defective proteostasis, and epigenetic alterations.

a Western bolt analysis for an expression protein by transfecting his-tagged NM_026333 in HEK293 cells. Total cell lysate of HEK293 cells transfected with (right) or without (left) his-tagged NM_026333. **b**. Protein-protein interaction of his-tagged recombinant NM_026333 protein and lysate of TG and HEK-293 cells. Protein binding to his-tagged recombinant NM_026333 protein was purified with TALON magnetic beads. NCX1: Na^{+}-Ca^{2+} exchanger 1, rNMP: Recombinant NM_026333 protein. Representative bands for Western blot were shown. Similar results were obtained in separate experiments. **c.** Effect of recombinant NM_026333 protein at 10^{-4}M for 48 hours on primary aging hallmarks of genomic instability (HP1α and emerin), defective proteostasis (LC3II and Atg7), and epigenetic alterations (H3K4me3) in TG cells (n=3, upper panel, * $p<0.05$ vs TG), and genomic instability (emerin), defective proteostasis (Atg7 and P62), and epigenetic alterations (H4K5ac) in HEK 293 cells under 24-hour 10^{-7}M CF6 stimulation (n=3, lower panel, * $p<0.05$ vs HEK+CF6). rNMP: Recombinant NM_026333 protein. **d.** Effect of 3-minute pre-incubation with recombinant NM_026333 protein at 10^{-4}M on 10^{-6}M acetylcholine-induced Ca^{2+} waveform in HEK293 cells. Representative Ca^{2+} waveforms were shown. Similar

results were obtained in separate three experiments.

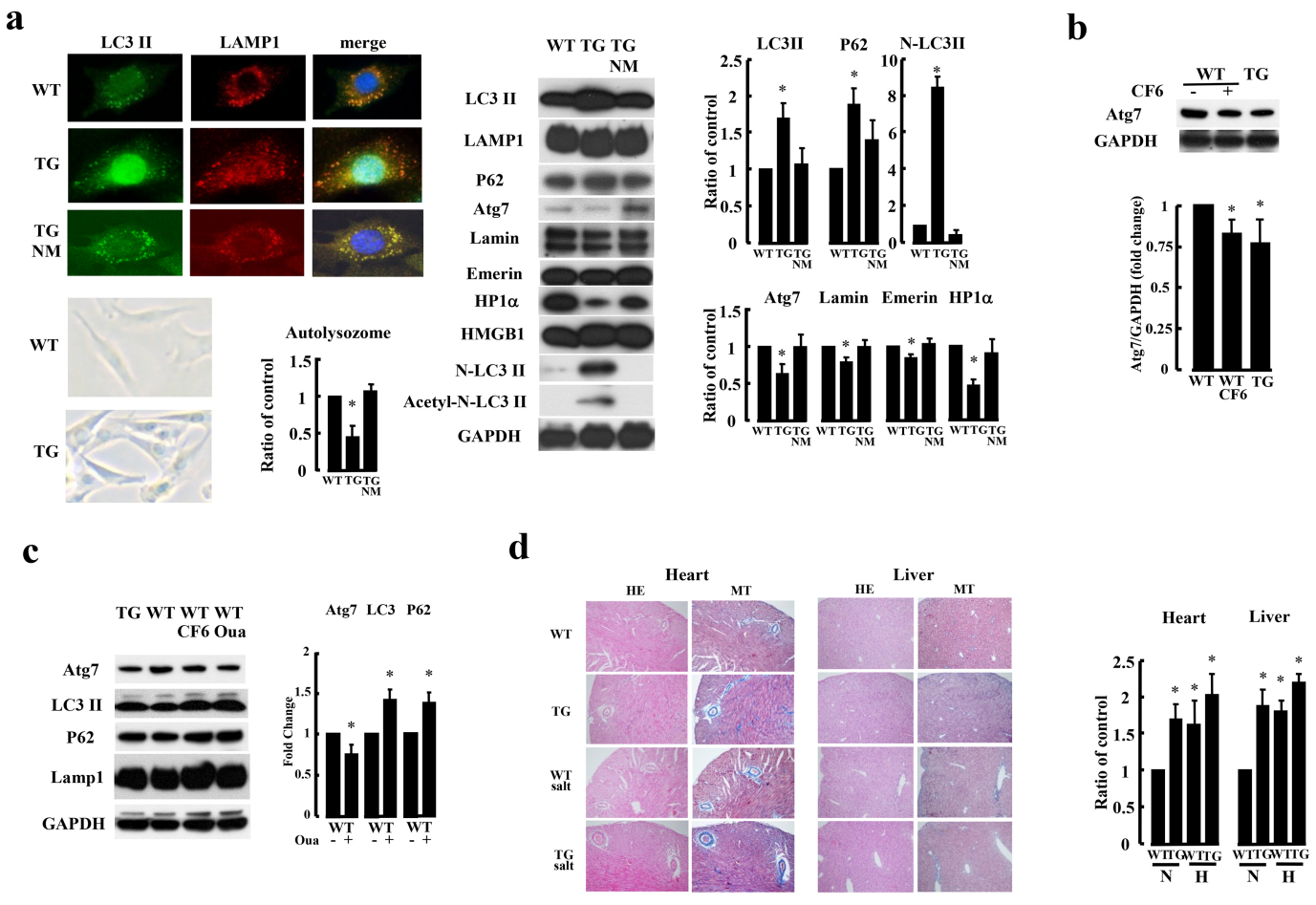
a
LC3 II
LAMP1
merge
WT
TG
TG NM
WT
TG
Autolysozome
Ratio of control
WT TG TG NM
WT TG TG NM
LC3 II
LAMP1
P62
Atg7
Lamin
Emerin
HP1α
HMGB1
N-LC3 II
Acetyl-N-LC3 II
GAPDH
LC3II
P62
N-LC3II
Ratio of control
Atg7
Lamin
Emerin
HP1α
b
WT TG
CF6 - +
Atg7
GAPDH
Atg7/GAPDH (fold change)
WT WT TG
CF6
c
TG WT WT WT
CF6 Oua
Atg7
LC3 II
P62
Lamp1
GAPDH
Atg7 LC3 P62
Fold Change
Oua - + - + - +
d
Heart
Liver
HE
MT
WT
TG
WT salt
TG salt
Heart
Liver
Ratio of control
N
H

Figure 1

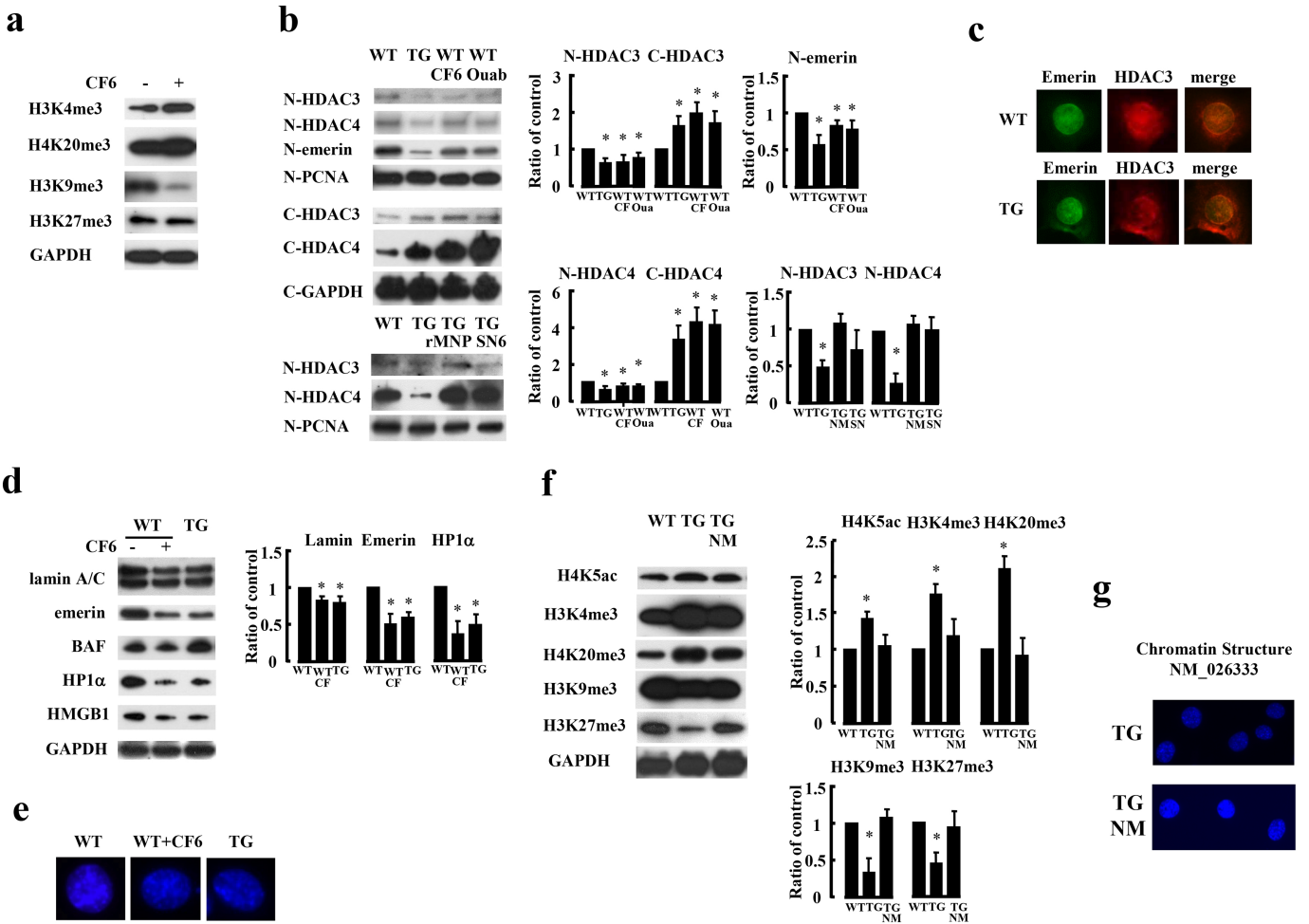
a
CF6 - +
H3K4me3
H4K20me3
H3K9me3
H3K27me3
GAPDH
b
WT TG WT WT CF6 Ouab
N-HDAC3
N-HDAC4
N-emerin
N-PCNA
C-HDAC3
C-HDAC4
C-GAPDH
WT TG TG TG rMNP SN6
N-HDAC3
N-HDAC4
N-PCNA
N-HDAC3 C-HDAC3
Ratio of control
WT TG WT WT CF Oua
N-emerin
N-HDAC4 C-HDAC4
N-HDAC3 N-HDAC4
WT TG TG TG NM SN
c
Emerin HDAC3 merge
WT
TG
d
WT TG
CF6 - +
lamin A/C
emerin
BAF
HP1α
HMGB1
GAPDH
Lamin Emerin HP1α
Ratio of control
WT WT TG CF
e
WT WT+CF6 TG
f
WT TG TG NM
H4K5ac
H3K4me3
H4K20me3
H3K9me3
H3K27me3
GAPDH
H4K5ac H3K4me3 H4K20me3
Ratio of control
WT TG TG NM
H3K9me3 H3K27me3
g
Chromatin Structure NM_026333
TG
TG NM

Figure 2

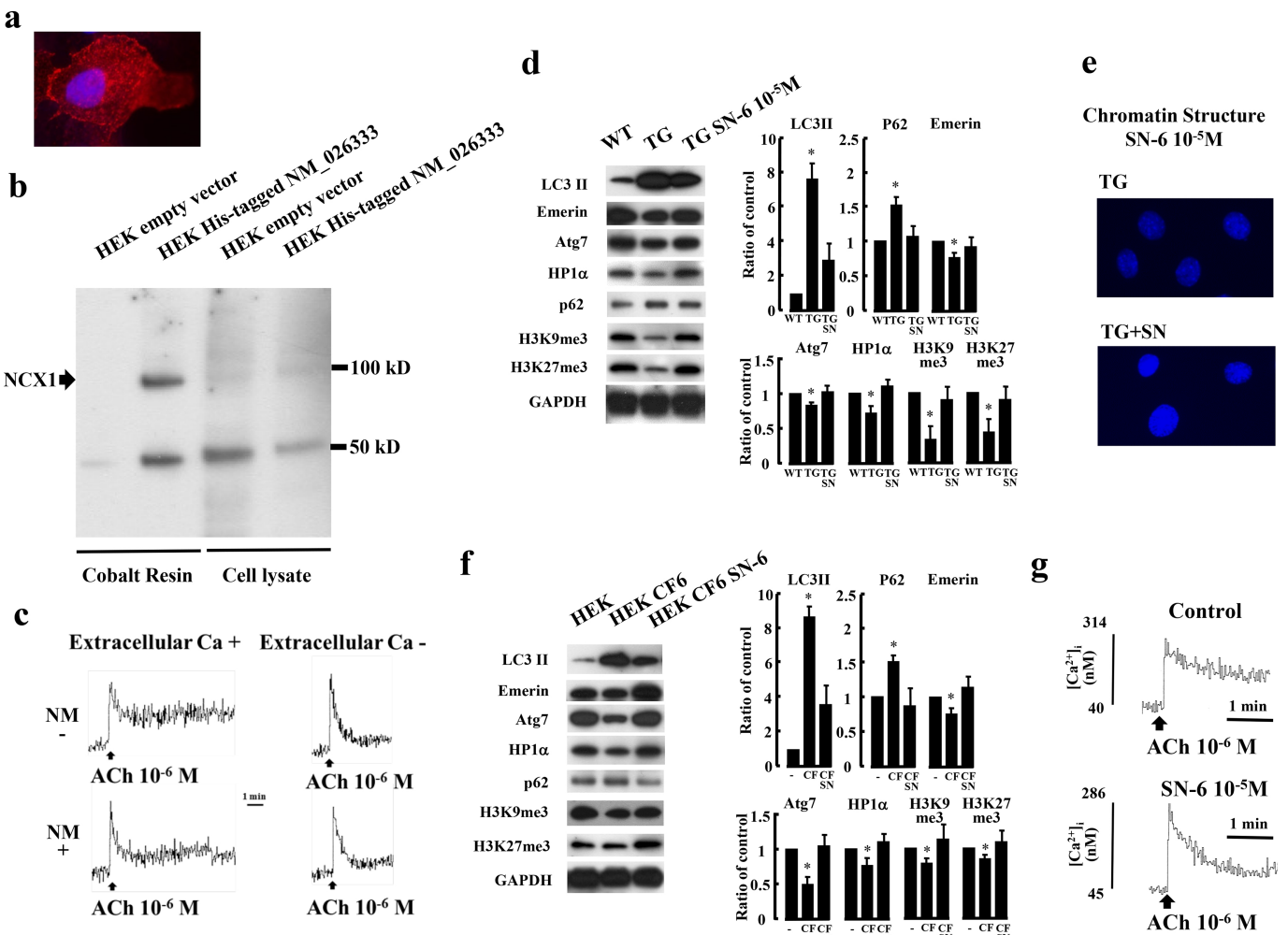
a
b
HEK empty vector
HEK His-tagged NM_026333
HEK empty vector
HEK His-tagged NM_026333
NCX1
100 kD
50 kD
Cobalt Resin
Cell lysate
c
Extracellular Ca +
Extracellular Ca -
NM -
NM +
ACh 10-6 M
1 min
d
WT
TG
TG SN-6 10-5M
LC3 II
Emerin
Atg7
HP1α
p62
H3K9me3
H3K27me3
GAPDH
LC3II
P62
Emerin
Ratio of control
Atg7
HP1α
H3K9 me3
H3K27 me3
e
Chromatin Structure
SN-6 10-5M
TG
TG+SN
f
HEK
HEK CF6
HEK CF6 SN-6
g
Control
SN-6 10-5M
[Ca2+]i (nM)
314
40
286
45
1 min
ACh 10-6 M

Figure 3

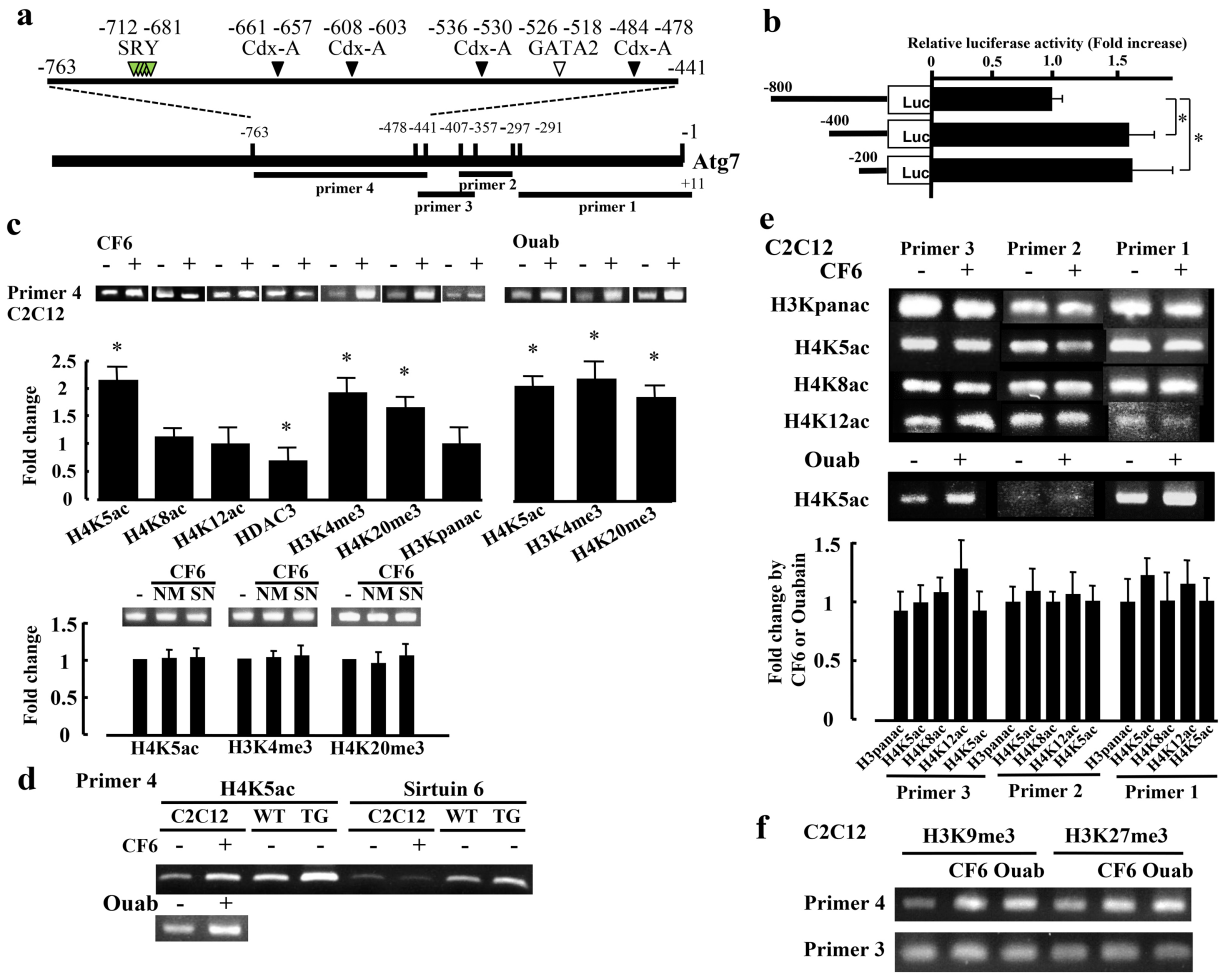
a
-712 -681
SRY
-661 -657
Cdx-A
-608 -603
Cdx-A
-536 -530
Cdx-A
-526 -518
GATA2
-484 -478
Cdx-A
-763
-441
-763
-478 -441 -407 -357 -297 -291
-1
Atg7
primer 4
primer 2
primer 3
primer 1
+11
b
Relative luciferase activity (Fold increase)
0
0.5
1.0
1.5
-800
-400
-200
Luc
Luc
Luc
*
*
c
CF6
Ouab
Primer 4
C2C12
Fold change
H4K5ac
H4K8ac
H4K12ac
HDAC3
H3K4me3
H4K20me3
H3Kpanac
H4K5ac
H3K4me3
H4K20me3
CF6
NM SN
Fold change
H4K5ac
H3K4me3
H4K20me3
d
Primer 4
H4K5ac
Sirtuin 6
C2C12
WT
TG
C2C12
WT
TG
CF6
Ouab
e
C2C12
Primer 3
Primer 2
Primer 1
CF6
H3Kpanac
H4K5ac
H4K8ac
H4K12ac
Ouab
H4K5ac
Fold change by CF6 or Ouabain
H3panac
H4K5ac
H4K8ac
H4K12ac
H4K5ac
Primer 3
Primer 2
Primer 1
f
C2C12
H3K9me3
H3K27me3
CF6 Ouab
CF6 Ouab
Primer 4
Primer 3

Figure 4

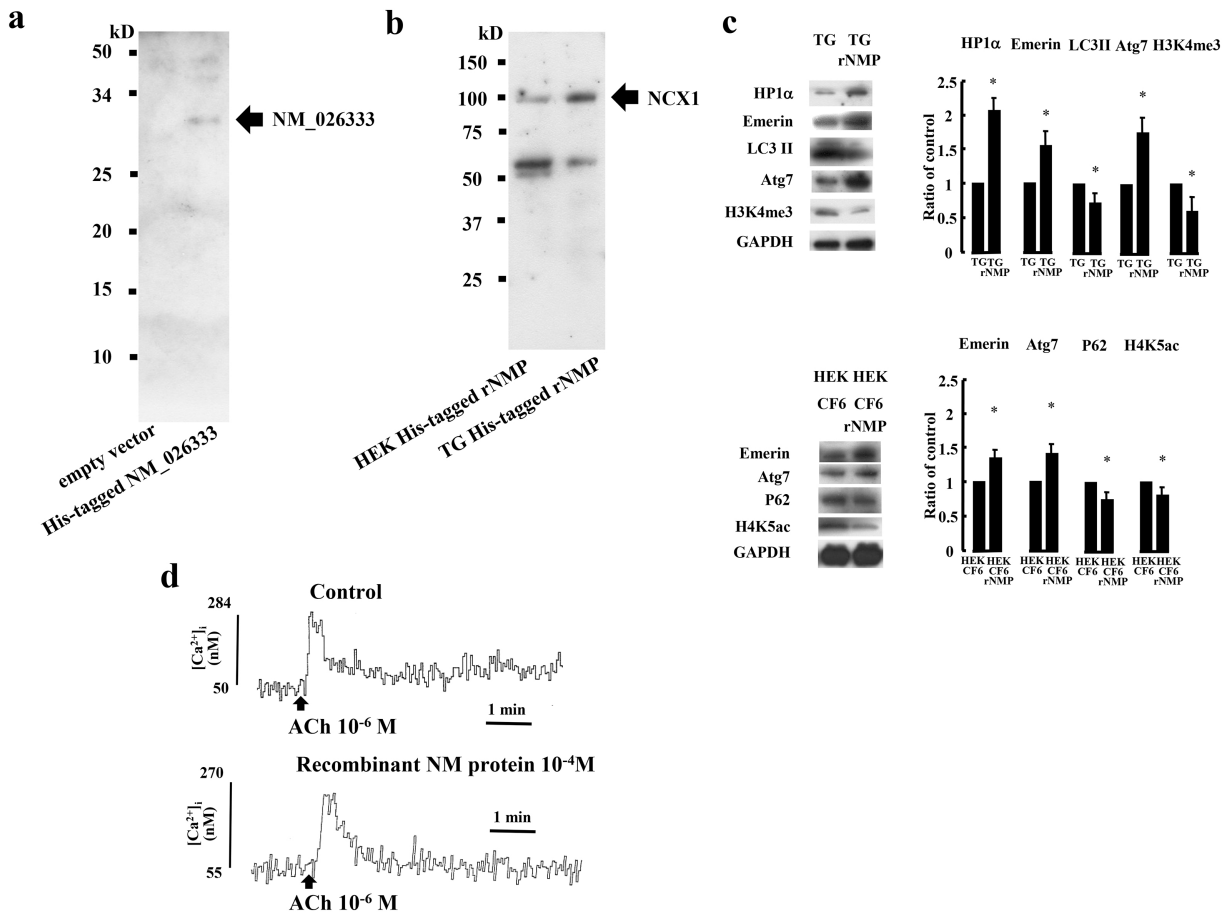
a
kD
50
34
25
20
15
10
NM_026333
empty vector
His-tagged NM_026333
b
kD
150
100
75
50
37
25
NCX1
HEK His-tagged rNMP
TG His-tagged rNMP
c
TG TG rNMP
HP1α
Emerin
LC3 II
Atg7
H3K4me3
GAPDH
HP1α Emerin LC3II Atg7 H3K4me3
Ratio of control
HEK HEK CF6 CF6 rNMP
Emerin
Atg7
P62
H4K5ac
GAPDH
Emerin Atg7 P62 H4K5ac
d
Control
284
50
[Ca2+]i (nM)
ACh 10-6 M
1 min
Recombinant NM protein 10-4M
270
55
ACh 10-6 M
1 min

Figure 5